Cu-releasing nanoparticles induce the catalytic transamination of amino acids and GSSG under tumor microenvironment conditions

Javier Bonet-Aleta[1,2,3,4], Juan Vicente Alegre-Requena[5], Javier Martin-Martin[1,6], Miguel Encinas-Gimenez[1,2,3,4], Ana Martín-Pardillos[1,2,4], Pilar Martin-Duque[3,4,7], Jose L. Hueso[1,2,3,4,], Jesus Santamaria[1,2,3,4,*]*

[1]Instituto de Nanociencia y Materiales de Aragon (INMA) CSIC-Universidad de Zaragoza, Campus Rio Ebro, Edificio I+D, C/ Poeta Mariano Esquillor, s/n, 50018, Zaragoza, (Spain).

[2]Department of Chemical and Environmental Engineering, University of Zaragoza, Campus Rio Ebro, C/María de Luna, 3, 50018 Zaragoza (Spain).

[3]Networking Res. Center in Biomaterials, Bioengineering and Nanomedicine (CIBER-BBN), Instituto de Salud Carlos III; 28029 Madrid (Spain)

[4] Instituto de Investigación Sanitaria (IIS) de Aragón, Avenida San Juan Bosco, 13, 50009 Zaragoza, Spain.

[5]Departamento de Química Inorgánica, Instituto de Síntesis Química y Catálisis Homogénea (ISQCH) CSIC-Universidad de Zaragoza, C/ Pedro Cerbuna 12, 50009 Zaragoza, Spain.

[6]Department of Organic Chemistry, University of Zaragoza, Zaragoza (Spain).

[7]Surgery Department, Medicine Medical School, University of Zaragoza, 50009 Zaragoza, Spain

KEYWORDS Copper, Amino acids, Transamination, Nanocatalysis, Cancer therapy, Glutathione, Glutamine, Alanine, Pyruvate.

Abstract

Catalytic cancer therapy is emerging as a powerful tool to target cancer cells by exploiting specific characteristics of the tumor microenvironment (TME). To this end, the catalytic activity of nanoparticles, enzymes and homogeneous catalysts is recruited to induce reactions that are damaging to cancer cells. Thus, the pro-drug activation approach uses chemical constructs that become toxic species inside the tumor, typically following removal of a protecting group. In contrast, TME-based catalytic strategies do not rely on the introduction of foreign species and instead use molecules that are already present in the TME. So far, only four processes have been explored in relation to cancer therapy, two oxidation reactions (glucose and glutathione), generation of reactive oxygen species (ROS) and production of oxygen to alleviate tumor hypoxia. This is surprising, since the rich chemical environment in tumor cells could in principle provide many other therapeutic opportunities. In particular, amino groups seem a suitable target, given the abundance of proteins and peptides in biological environments. Here we show that catalytic CuFe nanoparticles are able to foster transamination reactions between different amino acids and pyruvate, another key molecule that abounds in the TME. Transamination would then reduce the available aminoacid pool, which is likely to affect cell homeostasis and to effectively hinder tumor proliferation. After internalization of Cu-containing nanoparticles in U251-MG cells, we observed a significant decrease in glutamine and alanine levels up to 48 hours after treatment. In addition, we have found that not only simple amino acids, but also di- and tri-peptides undergo catalytic transamination when exposed to the Cu cations released by our nanoparticles, thus extending the range of the effects to other molecules such as GSSG. Mechanistic calculations for GSSG transamination revealed the formation of an imine between

the oxo-group of pyruvate and the free -NH_2 group of GSSG, followed by the coordination of the imine to Cu(II). Our results demonstrate that transamination reactions can be catalyzed *in cellulo* by Cu-releasing nanoparticles, adding a new reaction to the existing toolbox of catalytic therapies.

Introduction

Catalytic nanoparticles have recently been enlisted as new warriors in the fight against cancer. In particular, it is expected that they will help to modify the chemistry of the tumor microenvironment (TME), fostering tumor cell death or at least a non-proliferative scenario. Catalytic actions have followed two main strategies. The first corresponds to the so-called "pro-drug activation" approach that involves *in situ* production of chemotherapy drugs from less toxic or inert molecules, usually by metal-catalyzed chemical reactions[1] such as dealkylation[2], azide-alkyne cycloaddition[3] or carbamate cleavage[4] (***Figure 1a***). This has given rise to a vast array of possibilities, especially with de-protection chemistry, as researchers devised creative ways of anchoring inactive functional groups that could later be cleaved on site by the action of a metal catalyst[1, 5]. The second strategy, often termed "Nanocatalytic Therapy", exploits essential features of the Tumor Microenvironment (TME)[6-8] and in contrast to the pro-drug activation route, rather than introducing foreign molecules, attempts to do chemistry with the chemical species already available. Researchers in this field have displayed remarkable creativity in the search for nanostructured vectors that are more selective or more efficient in nanocatalytic therapy and this trend continues to this day,[9-12]. However, some stagnation is visible regarding the reactions and biomolecules to be targeted. In fact, the set of reactions employed for catalytic therapy has not changed in years, including only four processes, namely: (**i**) Glutathione (GSH) oxidation[13]; (**ii**)

Reactive Oxygen Species (ROS) production (H_2O_2, $\bullet O_2^-$ or •OH)[14, 15]; (**iii**) O_2 production using endogenous H_2O_2[16] and (**iv**) Glucose oxidation[17] (***Figure 1b***). These catalytic reactions are powerful tools to disrupt the tumor homeostasis by altering its redox balance (via processes **i-ii**), the typically hypoxic environment (via process **iii**), and nutrient supply (via process **iv**), respectively. Reactions **i**, **ii** and **iv** are oxygen-dependent and are therefore hampered under the hypoxic conditions of the TME. This is where reaction **iii** enters, aimed to alleviate hypoxia locally using available H_2O_2. These strategies interfere with cellular metabolism in general but are particularly harmful to cancer cells given their elevated oxidative stress[18] and dependency on glucose uptake[19]. *In vitro* and *in vivo* studies have analyzed potential effects on proteins, enzymes and genes involved in redox homeostasis whose functioning becomes altered by these catalytic processes, such as, Glutathione Peroxidase (GPX4)[20], dihydroorotate dehydrogenase (DHODH)[21] or Hypoxia-Induced Factor (HIF-1)[22] among others.

As already mentioned, the existing nanoparticle catalysts for catalytic therapy work exclusively around the four processes described in ***Figure 1b***, and no new reaction pathways have been reported. This is surprising since the TME is teeming with key molecules and reactions that could be exploited, and it seems unlikely that these four processes could exhaust all the catalytic opportunities available to fight cancer growth. Recently, Moran and coworkers[23,24] demonstrated that transamination, a reaction of biological importance that is usually governed by enzymatic catalysis, could also be catalyzed in a test tube by Co^{2+}, Ni^{2+}, V^{5+} and especially Cu^{2+} cations. Inspired by this work, we hypothesized that the use of Cu-releasing nanoparticles that are easily internalized by endocytosis and display a rapid Cu^{2+} release kinetics[25] could effectively perform this type of catalysis within cancer cells thus adding a new reaction to the panoply pictured in ***Figure 1b***. Specifically, we propose that the

catalytic action of transition metals on key molecules such as amino acids and α-ketoacids (***Figure 1c***) may open up unexplored therapeutic opportunities.

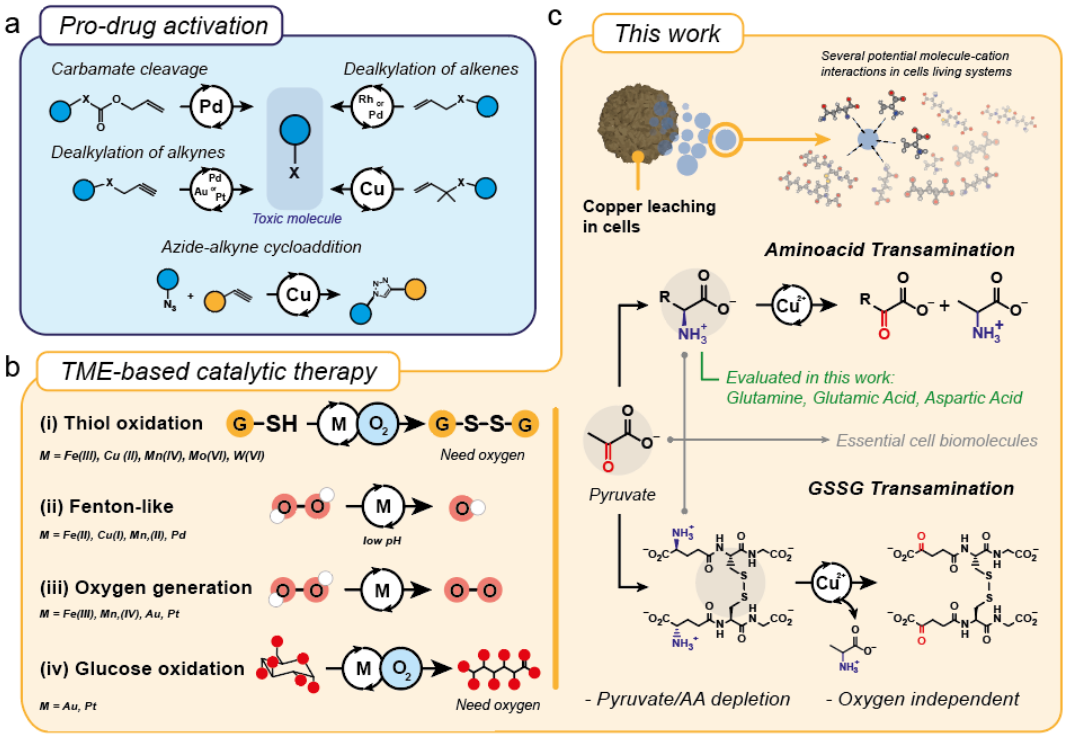

Figure 1. Different catalytic strategies developed for cancer therapy. (**a**) Bioorthogonal catalysis based on pro-drug activation strategies typically require a transition-metal catalyst including Pd, Pt, Au, Rh or Cu to form a cytotoxic compound by either removing a chemical group from a pro-drug or binding two low-toxicity molecules; (**b**) Reactions employed in the context of nanocatalytic therapy in the TME: (i) GSH oxidation, (ii) •OH or (iii) O_2 generation using endogenous H_2O_2 and (iv) glucose oxidation; (**c**) New scenario potentially enabled by the internalization of transition-metal leaching nanoparticles. In particular, Cu^{2+} catalyzes the transamination reaction between the $-NH_3^+$ group attached to α-C of an aminoacid/peptide and the keto group of pyruvate to yield D/L-Alanine and the corresponding keto-acid derived from the aminoacid/peptide. Reactions target key biomolecules in the cell: Glutamine, glutamic acid, aspartic acid, GSSG.

Especially noteworthy, in view of its potential therapeutic value, is the oxygen-independent character of the transamination processes, enabling them to take place within the hypoxic TME without the need to resort to complex oxygen-generation schemes. Cancer cells are particularly sensitive to the depletion of key molecules employed as building blocks to sustain the energetic and growth demands of their accelerated metabolism[26]. Amino acids are essential players in these metabolic routes and indeed, amino acid starvation is currently employed in the clinic to treat Acute lymphoblastic leukemia or Non-Hodgkin lymphoma by targeting Asparagine through the enzyme L-Asparaginase[27], while others like Glutamine, Arginine or Methionine are currently being explored in pre-clinical or clinical phases[28]. On the other hand, the role of pyruvate as a key molecule in cell metabolism does not need to be emphasized, as it provides energy through either through the Krebs cycle or lactic acid fermentation routes. Finally, as presented in ***Figure 1b***, glutathione (GSH) is rapidly becoming another therapeutic target due to its central role in balancing intracellular redox stress in cancer cells. As such has been targeted through thiol oxidation and is one of the emerging areas of therapeutic potential using transition-metal catalysis[13] to yield GSSG[12, 25] as the main reaction product, although this can be easily converted back into GSH through the action Glutathione Reductase[29] by using FAD^+, somewhat reducing the therapeutic effect of the oxidation. In contrast, the transamination process of ***Figure 1c*** could provide another, non-oxidative way, to deplete both GSH and GSSG pools since they have an iso-peptidic bond between the $-COO^-$ group from the side chain of the glutamate residue and the amino group from cysteine that is expected to be chemically able to undergo transamination.

Using $CuCl_2$ as Cu(II) source requires a previous reduction step into Cu(I)[30] to be internalized through the high-affinity Cu(I)-selective copper ion channel (CTR1)[31], which restricts the total copper uptake by cell. Instead, here we have used $CuFe_2O_4$ nanoparticles as reservoirs to deliver much larger amounts of Cu upon

internalization into U251-MG glioblastoma cells. Nanoparticle internalization typically occurs via endocytosis[32-34] and this enables higher internalization rates, as all metal atoms in a particle enter the cell simultaneously. In our case, the primary particle size of the $CuFe_2O_4$ nanoparticles is around 8 nm and the specific Cu intake in each internalization event is likely to be much larger, as in the culture medium the particles form 37 nm agglomerates, according to NTA results[25], i.e. in each endocytosis event all the Cu contained in 60-90 nanoparticles enter the cell simultaneously. On the other hand, specific Cu importers such as members of the Ctr1 family have evolved to maintain Cu homeostasis and therefore manage comparatively very low ion fluxes. This means that internalization of Cu-containing nanoparticles is much more efficient as a method to supply Cu to the cell. In fact agglomerates of $CuFe_2O_4$ nanoparticles are easily visible in confocal microscopy images after a few hours of incubation[35]. In this work, we investigate whether the Cu^{2+} cations leached from the nanoparticles, in addition to their known role of promoting GSH oxidation[25, 32], may also catalyze transamination reactions using pyruvate and different amino acids/peptides as targeted substrates. In addition, we have performed DFT calculations to provide a theoretical support to the catalytic outcomes observed and specifically to the variation of intracellular glutamine, as a key amino acid, together with alanine, as transamination reaction product. We also demonstrate a promising and non-previously reported specific transamination of GSH, thereby adding a new reaction that may target this antioxidant key for the regulation of redox homeostasis in cancer cells.

Results & Discussion

Catalytic transamination of single amino acids under TME conditions. Similar to the work of Mayer et al.[23] we first carried out kinetic studies of the removal of glutamine, glutamic acid and aspartic acid via transamination, although in this case

we used Cu-releasing nanoparticles as catalysts (**Figure 2**). Also, the reactions in our case were carried out in the presence of 5 mM of GSH, an expected intracellular concentration in tumor cells[32]. This is important because the presence of GSH promotes Cu^{2+} leaching, in a much larger extent than any of the amino acids tested in this work (***Figure S1***).

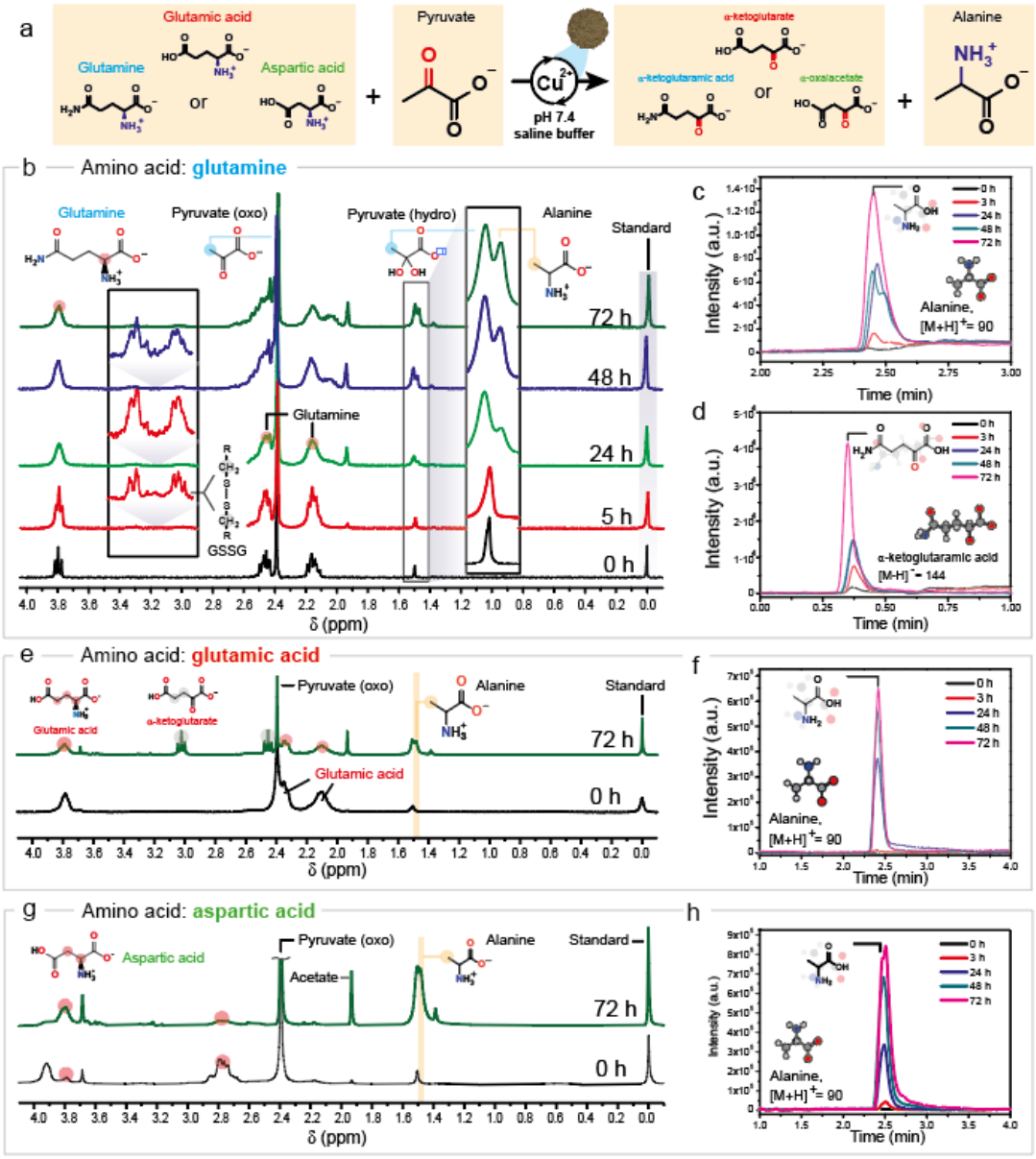

Figure 2. ^{1}H-NMR analysis of the transamination reaction in the presence of $CuFe_2O_4$ nanoparticles: (**a**) Schematic display of the transamination reaction between selected amino acids (glutamine, glutamic acid and aspartic acid acting as

amino-donors) and pyruvate to yield α-ketoacid acid and alanine; (**b**) ^{1}H-NMR analysis of the glutamine-pyruvate transamination reaction at different times; (**c-d**) UPLC-MS spectra of the amino-acid by-products of the glutamine-pyruvate transamination corresponding to alanine (m/z = 90, $[M+H]^{+}$) and α-ketoglutaramic acid (m/z = 144, $[M-H]^{-}$ respectively; (**e**) ^{1}H-NMR spectra of the glutamic acid-pyruvate transamination at different reaction time intervals; (**f**) UPLC-MS analysis of the increasing formation of alanine as by product of the glutamic acid-pyruvate transamination reaction (additional ^{1}H-NMR spectra and UPLC-MS chromatograms can be found in ***Figure S3*** and ***Figure S4***); Alanine derived from aspartic acid-pyruvate transamination reaction was also found in (**g**) ^{1}H-NMR spectra corresponding to the aspartic acid-pyruvate transamination at different reaction time intervals; (**h**) UPLC-MS analysis of alanine derived from aspartic acid-pyruvate transamination; (Additional ^{1}H-NMR spectra/UPLC-MS chromatograms are depicted in ***Figure S5*** and ***Figure S6***). Reaction conditions for all experiments: [Cu] = 6 mM, [Pyruvate] = 30 mM, [Amino acid] = 45 mM, [GSH] = 5 mM, pH = 7.4 (Na_2HPO_4/NaH_2PO_4 1M), T = 37 ºC.

Concerning the transamination of glutamine, under the catalysis of the leached Cu^{2+} cations the primary amine of glutamine (highlighted in blue, ***Figure 2a***) undergoes exchange with the keto-group of pyruvate (highlighted in red, ***Figure 2a***) yielding the corresponding α-ketoacid derived from the amino acid and alanine (***Figure 2a***) a reaction catalyzed by the released Cu^{2+} from the Cu-Fe nanoparticles[25]. It is noteworthy that this reaction is non-stereospecific[23] and consequently, the D-alanine generated as by-product (half of the total produced) becomes useless for cells. Therefore, the transamination reaction depicted in ***Figure 2a*** is potentially very useful for a catalytic starvation therapy scenario since it simultaneously removes glutamine and pyruvate, two key molecules in different types of cancers[36, 37], and can do so in an oxygen-independent fashion, therefore not being hampered by the

hypoxic conditions prevailing in the TME[38]. Next, we monitored the reaction of the $CuFe_2O_4$ nanoparticles with glutamine at different time intervals (***Figure 2b-d***). ^{1}H-NMR analysis at early reaction stages (5 h, ***Figure 2b***) revealed the characteristic signal of the generation of GSSG as by-product of the GSH oxidation[25, 39]. In contrast, we could not find the signal corresponding to alanine, suggesting that kinetics of Cu^{2+}-catalyzed GSH transformation into GSSG are faster in comparison to Cu^{2+}-catalyzed transamination reaction.

Longer reaction times resulted in an increase of the alanine signal (CH_3, 1.48 ppm, **Figure S2**), also detected by UPLC-MS (***Figure 2c***), and α-ketoglutaramic acid (***Figure 2d***), the α-ketoacid derived from glutamine. We also tested transamination with other important single amino acids, such as glutamic acid (***Figure 2e-f, Figure S3 and Figure S4***) and aspartic acid (***Figure 2g-h, Figure S5 and Figure S6***). The results were analogous to glutamine, ^{1}H-NMR and UPLC-MS analyses revealed a time-dependent increase of alanine and the corresponding α-ketoacid, (except for the case of the oxalacetate produced from aspartic acid which can be easily decarboxylated in the presence of transition metals such as Cu^{2+} (***Figure S5***)[40]), together with the depletion of pyruvate and the donor amino acid (***Figure S3-S6***). No alanine was found in the absence of the $CuFe_2O_4$ nanocatalyst (***Figure S7***). The efficiency of the reaction depended on the amino acid employed as substrate, with transamination yields in the order aspartic acid > glutamic acid > glutamine (***Figure S8***) in agreement with the results of Mayer et al.[23] using $CuCl_2$.

Beyond single amino acids: transamination of GSSG. We hypothesized that the same transamination investigated could extend beyond single amino acids to include peptides that possess free carboxyl ($–CO_2^–$) and amino ($–NH_3^+$) groups linked to the α-C atom of an amino acid residue. A very important example of this family of compounds would be GSH and its oxidized form GSSG. Both are peptides that exhibit this specific structural configuration (highlighted in orange in ***Figure 3a***).

Given their central role in redox homeostasis in cancer cells, transamination of these molecules could have significant interest in cancer therapy because the resulting unnatural α-ketoGSSG product might be more challenging for cancer cells to metabolize compared to naturally-occurring antioxidants like GSH and GSSG[41].

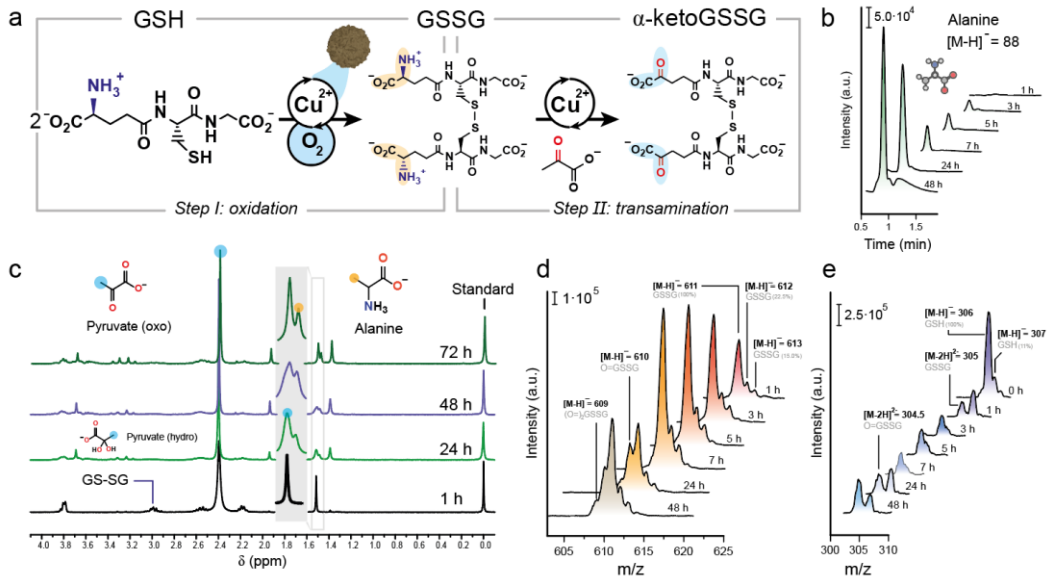

Figure 3. Cu-catalyzed transamination of GSH-GSSG in the presence of $CuFe_2O_4$ nanoparticles: (**a**) Cu^{2+} released from $CuFe_2O_4$ nanoparticles first catalyzes GSH oxidation with dissolved O_2, giving GSSG; then it furthers catalyzes its transamination with pyruvate; (**b**) UPLC-MS and (**c**) ^{1}H-NMR analysis of the generation of alanine from transamination of GSSG at different reaction times; (**d**, **e**) MS analysis of the formation of α-ketoGSSG and the depletion of GSH at various reaction times. Reaction conditions: [Cu] = 6 mM, [pyruvate] = 30 mM, [GSH] = 5 mM, pH = 7.4 (Na_2HPO_4/NaH_2PO_4 1 M), T = 37 ºC.

In the presence of O_2, the Cu^{2+}-catalyzed oxidation of GSH to GSSG exhibited faster kinetics than the competing transamination as can be seen at early reaction times (1 h), where UPLC-MS analysis revealed predominant generation of GSSG (***Figure 3d***) and depletion of GSH (***Figure 3e***), with minimal formation of alanine through transamination (***Figure 3b-c***). However, at longer reaction times (24 h and beyond),

the UPLC-MS, ^{1}H-NMR, and MS analyses detected the formation of alanine and α-ketoGSSG, demonstrating successful transamination of GSSG (***Figures 3b-d***). Additional experiments confirmed the compatibility of other polypeptides such as γ-Glu-ε-Lys with this transformation (***Figure S10***). Moreover, it was determined that amino acids containing secondary amines like proline were not subjected to transamination (***Figure S9***).

The transamination mechanism was investigated using density functional theory (DFT). Due to the presence of strong interactions among the different components, a direct evaluation of the Gibbs free energy difference (ΔG) between the isolated reagents and products did not yield informative results (***Figure S11***). Consequently, we used a comprehensive modeling approach that encompassed all pertinent reaction components, including GSSG/α-ketoGSSG, Cu^{2+}, pyruvate/alanine, and $HPO4^{2-}$, in the calculations illustrated in ***Figure 4***.

Initially, Cu^{2+} establishes strong interactions with the $-CO_2^-$ groups present in GSSG and pyruvate (**Int-I**, ***Figure 4d***). In the most stable conformation discovered, the cation predominantly coordinates with three $-CO_2^-$ groups, two of which stem from a folded branch of GSSG, and the other from pyruvate. Subsequently, one of the $-NH_3^+$ groups of GSSG reacts with the ketone of pyruvate, resulting in the formation of a protonated imine that needs/requires deprotonation before coordinating with Cu to generate **Int-II**. This sequence of steps exhibits slight endergonicity (ΔG = 4.1 kcal·mol^{-1}) when one of the $-CO_2^-$ groups acts as the base for deprotonation to obviate the need for separate calculations. Consistent with previous Cu-catalyzed transaminations[23], the calculated rate-limiting step involves the presence of the activated imine···Cu group. Therefore, the pH employed could influence the reaction kinetics, as a more alkaline solution would render deprotonation and subsequent imine···Cu coordination more favorable. This theoretical approach is supported by the observed roughly doubling of the reaction rate upon raising the pH from 5 to 9

(***Figure 4c***). Furthermore, the computational findings indicate that the transamination equilibrium is essentially energetically balanced (ΔG = 1.1 kcal·mol^{-1}, ***Figure 4d***), emphasizing the importance of an excess of pyruvate in the medium to drive the equilibrium towards the α-ketoGSSG product.

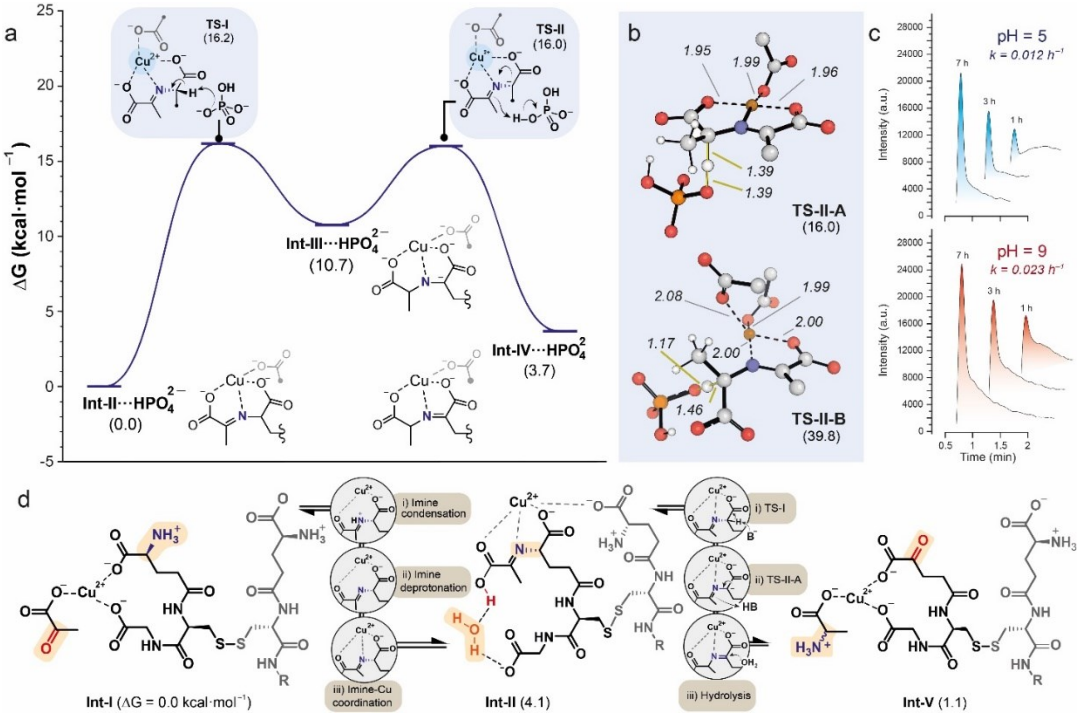

Figure 4. (**a**) ΔG values for the 1,3-H shift with HPO_4^{2-} acting as the H-transferring agent; (**b**) Depiction of the most stable conformers of **TS-II A** and **TS-II B** (dotted black lines indicate Cu–ligand bonds, thin yellow lines represent TS bonds, and distances are displayed in Å); (**c**) Experimental reaction rates at different pH values after 7 h; (**d**) Thermodynamic aspects of the transamination process. Computational protocols: DFT calculations[42-44] were carried out with ωB97X-D/Def2-QZVPP//ωB97X-D/6-31+G(d,p) [45-53], SMD[54-59] (solvent = water) was included in all the calculations, standard state = 1 M, T = 37 ºC [60].

Similar to previous mechanisms calculated for metal-catalyzed transaminations[23], the kinetics of the process are governed by a step-wise 1,3-H migration. In this mechanism, a HPO_4^{2-} basic molecule from the solution buffer triggers a H shift from

the α-C atom to the iminic C atom (***Figure 4a***). As in the imine-Cu coordination process, this base-promoted 1,3-H migration should be favored by more basic pH environments, which aligns with the experimental kinetic trend (***Figure 4c***). Interestingly, this process not only involves C=N···Cu activation but also CO_2^-···Cu activation of the $-CO_2^-$ group located next to the carbanion resulting from H abstraction. The Cu atom coordinates with this $-CO_2^-$ group, enhancing its capability to stabilize neighboring carbanions and thus reducing the energy barriers ($\Delta G^{\ddagger}$ from 39.8 to 16.0 kcal in **TS-II B** and **TS-II A**, respectively, ***Figure 4b***).

Intracellular transamination in U251-MG catalyzed by $CuFe_2O_4$ nanoparticles. Encouraged by the activity of lixiviated Cu^{2+} as a transamination catalyst for a variety of biologically relevant substrates, we evaluated the capability of $CuFe_2O_4$ nanoparticles to disrupt the amino acid pool in U251-MG cancer cells. We selected this cell line on the account of the significant role played by glutamine in their metabolism[61]. Indeed, some studies point out the relevance of glutamine in NADPH production and anaplerotic reactions (i.e. to generate Kreb's cycle intermediates) beyond their role as a nitrogen source in glioblastoma cells.[61] We detected a significant decrease in the intracellular glutamine levels in U251-MG cells incubated with the $CuFe_2O_4$ nanoparticles after 72 h (**Figure 5a**). On the other hand, intracellular alanine levels clearly increased for the $CuFe_2O_4$-treated group up to 48 h. This is consistent with the results shown above, as there is a significant pool of intracellular pyruvate and using pyruvate as the ketoacid always yielded alanine in all transamination reactions evaluated throughout this work, regardless of the amino-precursor. Interestingly, alanine was consumed both in the control and in the treated U251-MG cells (**Figure 5b**) at 72 h. We interpret this result as a consequence of cellular metabolic responses. In the absence of other amino acids, alanine can be incorporated into the TCA cycle to support ATP biosynthesis through its enzymatic transamination to pyruvate[62]. In addition, alanine can also serve as nitrogen source

in glutamine-starved glioblastoma cells[63]. Both of these facts may explain the strong decrease observed in both groups after 72 h. Finally, although only glutamine was monitored, our results show that the catalyst promotes transamination of a variety of amino-acids and peptides, causing a severe disruption of the cell metabolism.

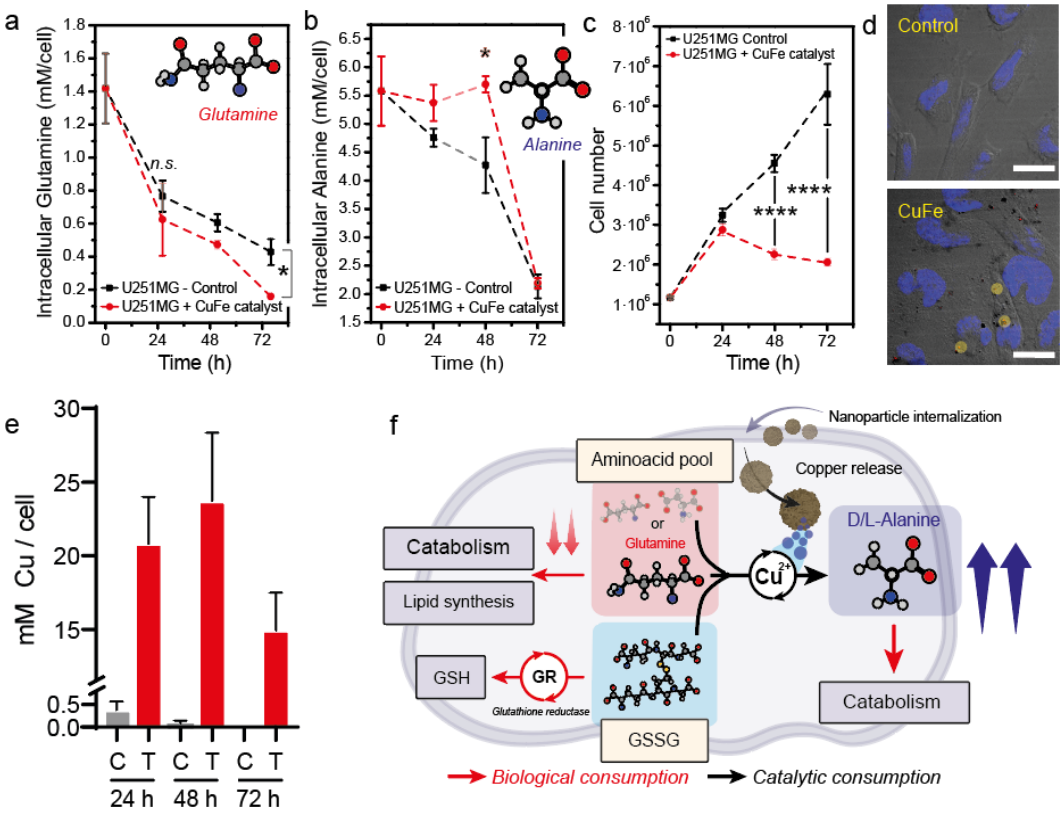

Figure 5. Tracking the intracellular transamination induced by $CuFe_2O_4$ nanoparticles. (**a**) Intracellular glutamine concentrations decrease for both control and treated U251-MG cells. Glutamine is a key metabolite for cells as one of the major Nitrogen sources and its used both for TCA cycle or fatty acid/nucleotide biosynthesis[64]. Treatment with $CuFe_2O_4$ nanoparticles significantly decreased glutamine levels especially after 72 h; (**b**) Monitoring intracellular alanine concentration revealed different profiles in control/treated U251-MG cells. After 24 and 48 h, the alanine concentration was significantly larger for treated U251 suggesting that artificial transamination had been successfully induced; (**c**) Cell growth stopped in the presence of $CuFe_2O_4$ nanoparticles, while it increased linearly

for the control sample; (**d**) Confocal microscopy analysis of U251-MG cells revealed the internalization of $CuFe_2O_4$ nanoparticles in the form of aggregates (highlighted in yellow); (**e**) Intracellular copper levels of U251-MG cells treated with 50 $\mu g \cdot mL^{-1}$ of $CuFe_2O_4$ showed a strong increase of copper concentration up to 48 h, followed by a decrease at 72h; (**f**) Schematic illustration of some possible catalytic pathways of intracellular aminoacid pool: glutamine (or other amino acids) can enter different metabolic routes to enable ATP or lipid biosynthesis. However, internalization of $CuFe_2O_4$ nanoparticles increases the intracellular concentration of Cu^{2+}, a catalyst that promotes artificial amino acid / pyruvate transamination, as well as that of other species with suitable chemical structure such as GSH and GSSG. For GSSG this reaction competes with the reduction of GSSG to GSH by glutathione reductase. Statistically significant differences were express as follows: *$p < 0.05$, **$p < 0.005$, ***$p < 0.0005$ and ****$p < 0.00005$.

This helps to explain the abrupt interruption seen in the growth of cells for the treatment (**Figure 5c**) after 24 h. The successful internalization of the $CuFe_2O_4$ nanocatalyst was confirmed by confocal microscopy (***Figure 5d***). Nanoparticle aggregates could be detected inside U251-MG cells due to their own reflection, close to the cellular nucleus stained in blue (***Figure 5d***). We also studied the evolution of total intracellular copper, the main homogeneous catalysts studied in this work, after the treatment with $CuFe_2O_4$ nanoparticles using microwave plasma atomic emission spectroscopy (MP-AES) (***Figure 5e***). The maximum intracellular copper value was reached at 48 h after the treatment with 50 $\mu g \cdot mL^{-1}$ of $CuFe_2O_4$, which is in agreement with the maximum concentration of intracellular alanine in treated U251-MG cells (***Figure 5b***). After 72 h, intracellular copper concentration decreased down to 14.5 mM, following cellular regulation mechanisms and excretion of nanoparticles via endosomes. However, 72 h gives ample time for Cu^{2+} to perform

catalysis using the amino acid pool or the cytosolic GSSG as amino donors, and the pyruvate as α-ketoacid to catalyze the transamination reaction (***Figure 5f***).

Conclusions

We have explored the catalytic activity of Cu derived from $CuFe_2O_4$ nanoparticles to catalyze reactions involving chemical species that are essential for cell metabolism and proliferation: amino acids, GSSG and pyruvate. Cu^{2+} cations released from Cu-Fe nanoparticles were able to catalyze transamination using glutamine, glutamic acid and aspartic acid as amino acid substrates under conditions relevant to TME (i.e. hypoxia and a 5 mM concentration of GSH). We have expanded the scope of transamination by demonstrating that tri- and dipeptides are also suitable substrates if a α-C with free $-COO^-$/$-NH_3^+$ group is present in their structure. The main candidate for this expanded transamination would be the GSH/GSSG tandem because of their central role to maintain homeostasis in the tumor microenvironment. We have shown experimentally that the reaction proceeds in GSSG and explained it through in-depth mechanistic studies as a result of the formation of an imine between the oxo-group of pyruvate and the free $-NH_2$ group of GSSG, followed by the coordination of the imine to Cu(II). Finally, we have also shown that Cu-Fe nanoparticles could drive transamination reactions *in cellulo*. Internalization of Cu-Fe nanoparticles guarantees a high concentration of Cu within U251-MG cells for at least 48 h. As a result, glutamine consumption is accelerated while intracellular alanine levels rise and cell proliferation abruptly stops, a scenario in good agreement with transamination reactions catalyzed by Cu(II)-releasing nanoparticles. In summary, the results of this work establish copper-catalyzed transamination as a new valuable reaction to be added to the existing toolkit of TME-based nanocatalytic therapy.

METHODS

Chemicals. L-Glutamine (ReagentPlus®, ≥99% (HPLC)), L-Glutamic Acid (ReagentPlus®, ≥99% (HPLC)), L-Aspartic Acid (ReagentPlus®, ≥99% (HPLC)), L-Alanine (ReagentPlus®, ≥99% (HPLC)), L-Proline (ReagentPlus®, ≥99% (HPLC)), L_Glutathione reduced (≥98%), γ-Glu-ε-Lys (≥98.0% (TLC)), Sodium pyruvate (ReagentPlus®, ≥99%), Iron(III) chloride hexahydrate ($FeCl_3 \cdot 6H_2O$, 97%), copper(II) chloride dihydrate ($CuCl_2 \cdot 2H_2O$, 99.0%), sodium acetate anhydrous (CH_3COONa, 99.0%), bovine serum albumin (BSA), ethylene glycol (EG), dimercaptosuccinic acid (DMSA, 99.0%), Na_2HPO_4, NaH_2PO_4, $(CH_3)_3SiCD_2CD_2CO_2Na$ (98% atom D), Chelex resin were purchased from Sigma-Aldrich and were used without further purification. Acetonitrile (HPLC quality) was purchased from VWR chemicals. Dulbecco's modified Eagle's medium (DMEM, Biowest, France) cell culture medium was supplemented with 10% of Fetal Bovine Serum (FBS, GIBCO, USA) and 1% penicillin/streptomycin and 1% amphotericin (Biowest, France)

Synthesis of the copper-iron oxide nanocatalyst. $CuFe_2O_4$ nanoparticles were prepared following our previous methodologies[25].

^{1}H-NMR analysis of reaction. General procedure. Pyruvate, Aminoacid, Glutathione (GSH) and $CuFe_2O_4$ nanoparticles were added to a sealed vial up to reach a final concentration of 30 mM, 45 mM, 5 mM and 6 mM (expressed in [Cu]), respectively in 10 mL of 1 M Na_2HPO_4/NaH_2PO_4. Prior to the addition of nanoparticles, O_2 was removed from solution using Ar. Finally, temperature was set up to 37 ºC.

For analysis, 1 mL of the sample was collected with a syringe and further filtered using a 0.22 µm Nylon filter. The resulting solution was incubated with 400 mg of Chelex resin for 30 minutes to remove metal ions to avoid paramagnetism in NMR. Then, 50 µL of D_2O containing 20.76 mM of $(CH_3)_3SiCD_2CD_2CO_2Na$ as internal

standard, were mixed with 550 µL of the previous solution and were analyzed using a Bruker Avance III 300 spectrometer (Bruker, Billerica, MA, USA) operating at 300 MHz proton frequency. Quantification of produced alanine was carried out using MestRenova software by integrating -CH_3 peak of alanine and normalizing it to 1.76 mM of the internal standard ($(CH_3)_3SiCD_2CD_2CO_2Na$).

UPLC-MS analysis of reaction. General procedure for all AA except GSH and γ-Glu-ε-Lys. Pyruvate, Aminoacid, Glutathione (GSH) and Cu-Fe nanoparticles were added to a sealed vial up to reach a final concentration of 30 mM, 45 mM, 5 mM and 6 mM (expressed in [Cu]), respectively in 2 mL of 1 M Na_2HPO_4/NaH_2PO_4. Specifically, for γ-Glu-ε-Lys concentrations employed were x4 times lower (i.e. [γ-Glu-ε-Lys] = 11.25 mM, [Pyruvate] 7.5 mM, [GSH] = 1.25 mM and [Cu] = 1.5 mM) Prior to the addition of nanoparticles, O_2 was removed from solution using Ar. Finally, temperature was set up to 37 ºC.

For analysis, 50 µL of the sample were collected with a syringe and diluted in 50 µL of miliQ H_2O. 5 µL of the previous solution were diluted in 995 µL of H_2O:Acetonitrile mixture. Resulting solution was filtered and analyzed using a Waters ACQUITY system H-Class coupled to a single quadrupole mass spectrometer with an electrospray ionization (ESI) ACQUITY QDa mass detector. Data acquisition and processing were performed by using MASSLYNX software (Waters Corporation USA). Chromatographic separation was performed using an ACQUITY UPLC BEH Amide column (130 A, 1.7 u, 2.1 mm x 100 mm, Waters). Mobile phase consisted of an initial mixture of Acetonitrile:H_2O (90:10) at a flow rate 0.5 mL/min, 85 ºC. H_2O composition increased for 3 min until a 65% acetonitrile is reached and then system can recover initial conditions. For analysis of GSH and γ-Glu-ε-Lys reactions, a mobile phase employed was a constant Acetonitrile:H_2O (65:35) at a constant flow rate 0.5 mL/min, 85ºC.

Intracellular analysis of Glutamine and alanine. $8 \cdot 10^5$ U251 cells were seeded onto P100 dishes. After 24 h, cell media was replaced with DMEM (10% FBS, 1% penicillin/streptomycin and 1% amphotericin) supplemented with $CuFe_2O_4$ nanoparticles (0.05 $mg \cdot mL^{-1}$) for treated cells and left incubated for 24h, 48h or 72h, respectively. Then, cells were washed twice with PBS, trypsinized (5 minutes, 37ºC 5% CO_2), centrifuged (300g, 5') and washed again twice with ice-cold PBS (150 rpm , 5'). Finally, cell pellet was resuspended in 300 µL of mili-Q H_2O and ultrasonicated for 30' to ensure a correct cell lysis. Sample for UPLC-MS analysis was prepared by mixing 50 µL of the resulting solution with 950 µL of H_2O:ACN mixture (1:1). All samples were filtered with 0.22 mm w/w PFTE filters before injection in UPLC system. Chromatographic separation was performed using an ACQUITY UPLC BEH Amide column (130 A, 1.7 u, 2.1 mm x 100 mm, Waters). Mobile phase consisted of an initial mixture of Acetonitrile:H_2O (90:10) at a flow rate 0.5 mL/min, 85 ºC. H_2O composition increased for 3 min until a 65% acetonitrile is reached and then system can recover initial conditions.

Analysis of $CuFe_2O_4$ internalization by confocal microscopy. Confocal microscopy assay was carried out to assess the capacity of internalization of $CuFe_2O_4$ NPs into U251-MG. Cells were seeded onto 12 mm Ø coverslips, which were deposited on a 24-well plate, at a density of 20 000 cells per well, and incubated at 37 ºC and 5% CO_2. After 24 h, cells were treated with $CuFe_2O_4$ NPs dispersed in DMEM at a concentration of 25 $\mu g \cdot mL^{-1}$ during 24 h (for negative control wells, DMEM was replaced with fresh media). After this time, cells were washed 3 times with DPBS, fixed with 4% paraformaldehyde, and then washed 3 more times with DPBS. In order to prepare the samples for confocal microscopy, cells were permeabilized with 0.1% saponine. After that, samples were deposited onto a drop of Fluoromount-G + DAPI for nuclei staining. Nanoparticle aggregates could be observed due to the reflection of the incident light. To confirm the presence of the

nanoparticles inside the cell, a Z-Stack assay of the whole cell, and its ulterior maximum orthogonal projection were performed. This assay was carried out in a confocal microscope (ZEISS LSM 880 Confocal Microscope), using a 63x/1.4 Oil DIC M27 objective.

Quantification of intracellular copper. In a 6 well-plate, $2 \cdot 10^5$ cells per well were seeded and incubated at 37ºC under an atmosphere of 5% CO_2 for 24 h. Then, the cell culture medium was replaced by a dispersion of $CuFe_2O_4$ nanoparticles in DMEM with a final concentration of 50 $\mu g \cdot mL^{-1}$. To analyze the internalized copper, cells were detached using a 0.25% Trypsin (X0915-100, Biowest, France) solution in PBS, centrifuged at 6700 g for 5 minutes. The cell pellet was digested with Aqua Regia ($HCl \cdot HNO_3$ 3:1, v/v) overnight and analyzed with an Agilent 4100 MP-AES (Agilent, USA). All samples were filtered using a 0.22 µm nylon filter before their analysis.

Statistical analysis. All the results are expressed as mean ± S.E.M. Statistical analysis of the biological experiments and the significant differences among the means were evaluated by t-test using GraphPad Software). Statistically significant differences were express as follows: *p < 0.05, **p < 0.005, ***p < 0.0005 and ****p < 0.00005.

Computational methods. The ωB97X-D[46]/6-31+G(d,p)[47] combination was employed to optimize the geometries of stationary points. This functional has a track record of retrieving accurate geometries for systems with non-covalent interactions, such as hydrogen bonds[46,65]. To confirm that the optimized geometries were either energy minima or transition states, vibrational frequency calculations were carried out, generating vibrational information to calculate thermochemistry data using *GoodVibes*. Electronic energies were refined using single point energy corrections at the ωB97X-D/Def2-QZVPP[52] level. Furthermore, solvent effects were considered

in all calculations using the integral equation formalism variant of the polarizable continuum model (IEF-PCM) with the SMD solvation model (solvent = water)[59].

Gaussian 16[42] was used to run all the density functional theory (DFT) calculations. *AQME*[43] was employed to i) generate conformers (program = RDKit)[44], ii) identify and correct errors from geometry optimization and frequency DFT calculations, iii) remove duplicates, and iv) generate input files for single-point corrections in an automated manner (the command lines and input CSV file used are included in the ESI). Molecular representations were created using *PyMOL*[66] with the display settings developed by Dr. Robert S. Paton from Colorado State University, which are openly accessible [67].

The calculated vibrational entropies were corrected using quasi-harmonic (QHA) corrections, with a frequency cut-off value of 100.0 cm^{-1}, as proposed by Grimme[68]. This correction was performed using the *GoodVibes*[60] program at a temperature of 310.15 K (37 °C). In addition, a correction for the change in standard state from gas phase at 1 atm to a 1 M solution was introduced using the "-c 1" option in *GoodVibes*. The single point energies from ωB97X-D/Def2-QZVPP were corrected using the G corrections computed with ωB97X-D/6-31+G(d,p) to obtain the final G values. This correction was performed using the "--spc SUFFIX" option in *GoodVibes*. All the conformers were considered to calculate the reported Boltzmann-weighted G values of the different reaction steps using the "--pes FILENAME.yaml" option in *GoodVibes*. All these thermochemical values were tabulated in a separate file of the ESI. Automating the generation of G profiles helped us avoid potential errors resulting from manual manipulation of the data.

AUTHOR INFORMATION

Corresponding Author

*Jesus Santamaria, jesus.santamaria@unizar.es

*José Luis Hueso, jlhueso@unizar.es

Author Contributions

J.B.-A. and J. L. H. prepared and characterized the nanoparticles. J. B.-A. and J. M. M. performed ^{1}H-NMR experiments. J.B-A., A. M. P. and M. E. G. performed in vitro experiments. J.V. carried out quantum mechanical calculations. J. B.-A., J.V., M.P., L.O., J. L. H. and J.S. designed research. J. B.-A., J.L.H. and J.S. wrote the manuscript. All authors have contributed and given approval to the final version of the manuscript.

Funding Sources

Authors thanks the financial support from the European Research Council (ERC) Advanced Grant CADENCE number 742684. J.V.A.-R. acknowledges Gobierno de Aragón-Fondo Social Europeo (Research Group E07_23R) and the State Research Agency (AEI) of Spain for financial support through a Juan de la Cierva Incorporación contract (reference: IJC2020-044217-I). J.V.A.-R. acknowledges the computing resources at the Galicia Supercomputing Center, CESGA, including access to the FinisTerrae supercomputer, the Red Española de Supercomputación (grant number QH-2023-1-0003) and the Drago cluster facility of SGAI-CSIC.

Acknowledgments

J.B-A. acknowledges the Spanish Government for an FPU predoctoral contract. The TEM measurements were conducted at the Laboratorio de Microscopias Avanzadas, Instituto de Nanociencia y Materiales de Aragon, Universidad de Zaragoza, Spain. The synthesis of materials has been performed by the Platform of

Production of Biomaterials and Nanoparticles of the NANBIOSIS ICTS, more specifically by the Nanoparticle Synthesis Unit of the CIBER in BioEngineering, Biomaterials & Nanomedicine (CIBER-BBN).

References

1. Sousa-Castillo, A.; Mariño-López, A.; Puértolas, B.; Correa-Duarte, M. A., Nanostructured Heterogeneous Catalysts for Bioorthogonal Reactions. *Angewandte Chemie International Edition* **2023,** *62* (10), e202215427.
2. Pérez-López, A. M.; Rubio-Ruiz, B.; Sebastián, V.; Hamilton, L.; Adam, C.; Bray, T. L.; Irusta, S.; Brennan, P. M.; Lloyd-Jones, G. C.; Sieger, D.; Santamaría, J.; Unciti-Broceta, A., Gold-Triggered Uncaging Chemistry in Living Systems. *Angewandte Chemie International Edition* **2017,** *56* (41), 12548-12552.
3. Clavadetscher, J.; Hoffmann, S.; Lilienkampf, A.; Mackay, L.; Yusop, R. M.; Rider, S. A.; Mullins, J. J.; Bradley, M., Copper Catalysis in Living Systems and In Situ Drug Synthesis. **2016,** *55* (50), 15662-15666.
4. Chen, Z.; Li, H.; Bian, Y.; Wang, Z.; Chen, G.; Zhang, X.; Miao, Y.; Wen, D.; Wang, J.; Wan, G.; Zeng, Y.; Abdou, P.; Fang, J.; Li, S.; Sun, C.-J.; Gu, Z., Bioorthogonal catalytic patch. *Nature Nanotechnology* **2021,** *16* (8), 933-941.
5. Liang, T.; Chen, Z.; Li, H.; Gu, Z., Bioorthogonal catalysis for biomedical applications. *Trends in Chemistry* **2022,** *4* (2), 157-168.
6. Huo, M.; Wang, L.; Wang, Y.; Chen, Y.; Shi, J., Nanocatalytic Tumor Therapy by Single-Atom Catalysts. *ACS Nano* **2019,** *13* (2), 2643-2653.
7. Yang, B.; Chen, Y.; Shi, J., Nanocatalytic Medicine. *Advanced Materials* **2019,** *31* (39), 1901778.
8. Liu, P.; Huo, M.; Shi, J., Nanocatalytic Medicine of Iron-Based Nanocatalysts. **2021,** *3* (2), 2445-2463.
9. Lin, L.-S.; Song, J.; Song, L.; Ke, K.; Liu, Y.; Zhou, Z.; Shen, Z.; Li, J.; Yang, Z.; Tang, W.; Niu, G.; Yang, H.-H.; Chen, X., Simultaneous Fenton-like Ion Delivery and Glutathione Depletion by MnO2-Based Nanoagent to Enhance Chemodynamic Therapy. *Angewandte Chemie International Edition* **2018,** *57* (18), 4902-4906.
10. Ma, B.; Wang, S.; Liu, F.; Zhang, S.; Duan, J.; Li, Z.; Kong, Y.; Sang, Y.; Liu, H.; Bu, W.; Li, L., Self-Assembled Copper–Amino Acid Nanoparticles

for in Situ Glutathione “AND” H2O2 Sequentially Triggered Chemodynamic Therapy. *Journal of the American Chemical Society* **2019,** *141* (2), 849-857.

11. Meng, X.; Li, D.; Chen, L.; He, H.; Wang, Q.; Hong, C.; He, J.; Gao, X.; Yang, Y.; Jiang, B.; Nie, G.; Yan, X.; Gao, L.; Fan, K., High-Performance Self-Cascade Pyrite Nanozymes for Apoptosis–Ferroptosis Synergistic Tumor Therapy. *ACS Nano* **2021,** *15* (3), 5735-5751.

12. Wang, D.; Wu, H.; Wang, C.; Gu, L.; Chen, H.; Jana, D.; Feng, L.; Liu, J.; Wang, X.; Xu, P.; Guo, Z.; Chen, Q.; Zhao, Y., Self-Assembled Single-Site Nanozyme for Tumor-Specific Amplified Cascade Enzymatic Therapy. *Angewandte Chemie International Edition* **2021,** *60* (6), 3001-3007.

13. Xiong, Y.; Xiao, C.; Li, Z.; Yang, X., Engineering nanomedicine for glutathione depletion-augmented cancer therapy. *Chemical Society Reviews* **2021,** *50* (10), 6013-6041.

14. Yang, B.; Chen, Y.; Shi, J., Reactive Oxygen Species (ROS)-Based Nanomedicine. *Chemical Reviews* **2019,** *119* (8), 4881-4985.

15. Tang, Z.; Zhao, P.; Wang, H.; Liu, Y.; Bu, W., Biomedicine Meets Fenton Chemistry. *Chemical Reviews* **2021,** *121* (4), 1981-2019.

16. Szatrowski, T. P.; Nathan, C. F. J. C. r., Production of large amounts of hydrogen peroxide by human tumor cells. **1991,** *51* (3), 794-798.

17. Wang, C.; Yang, J.; Dong, C.; Shi, S., Glucose Oxidase-Related Cancer Therapies. *Advanced Therapeutics* **2020,** *3* (10), 2000110.

18. Hayes, J. D.; Dinkova-Kostova, A. T.; Tew, K. D., Oxidative Stress in Cancer. *Cancer cell* **2020,** *38* (2), 167-197.

19. Liberti, M. V.; Locasale, J. W., The Warburg Effect: How Does it Benefit Cancer Cells? *Trends in biochemical sciences* **2016,** *41* (3), 211-218.

20. Wu, C.; Liu, Z.; Chen, Z.; Xu, D.; Chen, L.; Lin, H.; Shi, J., A nonferrous ferroptosis-like strategy for antioxidant inhibition-synergized nanocatalytic tumor therapeutics. *Science advances* **2021,** *7* (39), eabj8833.

21. Chen, S.; Yang, J.; Liang, Z.; Li, Z.; Xiong, W.; Fan, Q.; Shen, Z.; Liu, J.; Xu, Y., Synergistic Functional Nanomedicine Enhances Ferroptosis Therapy for Breast Tumors by a Blocking Defensive Redox System. *ACS Applied Materials & Interfaces* **2023,** *15* (2), 2705-2713.

22. Sun, Y.; Zhou, Z.; Yang, S.; Yang, H., Modulating hypoxia inducible factor-1 by nanomaterials for effective cancer therapy. *WIREs Nanomedicine and Nanobiotechnology* **2022,** *14* (1), e1766.

23. Mayer, R. J.; Kaur, H.; Rauscher, S. A.; Moran, J., Mechanistic Insight into Metal Ion-Catalyzed Transamination. *Journal of the American Chemical Society* **2021,** *143* (45), 19099-19111.

24. Dherbassy, Q.; Mayer, R. J.; Muchowska, K. B.; Moran, J., Metal-Pyridoxal Cooperativity in Nonenzymatic Transamination. *Journal of the American Chemical Society* **2023**.

25. Bonet-Aleta, J.; Encinas-Gimenez, M.; Urriolabeitia, E.; Martin-Duque, P.; Hueso, J. L.; Santamaria, J., Unveiling the interplay between homogeneous and heterogeneous catalytic mechanisms in copper–iron nanoparticles working under chemically relevant tumour conditions. *Chemical Science* **2022,** *13* (28), 8307-8320.

26. Vander Heiden, M. G.; Cantley, L. C.; Thompson, C. B., Understanding the Warburg effect: the metabolic requirements of cell proliferation. *Science (New York, N.Y.)* **2009,** *324* (5930), 1029-33.

27. Butler, M.; van der Meer, L. T.; van Leeuwen, F. N., Amino Acid Depletion Therapies: Starving Cancer Cells to Death. *Trends in endocrinology and metabolism: TEM* **2021,** *32* (6), 367-381.

28. DeBerardinis, R. J.; Chandel, N. S., Fundamentals of cancer metabolism. **2016,** *2* (5), e1600200.

29. Fagan, R. L.; Palfey, B. A., 7.03 - Flavin-Dependent Enzymes. In *Comprehensive Natural Products II*, Liu, H.-W.; Mander, L., Eds. Elsevier: Oxford, 2010; pp 37-113.

30. Ohgami, R. S.; Campagna, D. R.; McDonald, A.; Fleming, M. D., The Steap proteins are metalloreductases. *Blood* **2006,** *108* (4), 1388-94.

31. Chen, L.; Min, J.; Wang, F., Copper homeostasis and cuproptosis in health and disease. *Signal Transduction and Targeted Therapy* **2022,** *7* (1), 378.

32. Bonet-Aleta, J.; Sancho-Albero, M.; Calzada-Funes, J.; Irusta, S.; Martin-Duque, P.; Hueso, J. L.; Santamaria, J., Glutathione-Triggered catalytic response of Copper-Iron mixed oxide Nanoparticles. Leveraging tumor microenvironment conditions for chemodynamic therapy. *Journal of Colloid and Interface Science* **2022,** *617*, 704-717.

33. Wang, Z.; Li, N.; Zhao, J.; White, J. C.; Qu, P.; Xing, B., CuO Nanoparticle Interaction with Human Epithelial Cells: Cellular Uptake, Location, Export, and Genotoxicity. *Chemical Research in Toxicology* **2012,** *25* (7), 1512-1521.

34. Rennick, J. J.; Johnston, A. P. R.; Parton, R. G., Key principles and methods for studying the endocytosis of biological and nanoparticle therapeutics. *Nature Nanotechnology* **2021,** *16* (3), 266-276.

35. Bonet-Aleta, J.; Sancho-Albero, M.; Calzada-Funes, J.; Irusta, S.; Martin-Duque, P.; Hueso, J. L.; Santamaria, J., Glutathione-Triggered catalytic response of Copper-Iron mixed oxide Nanoparticles. Leveraging tumor microenvironment conditions for chemodynamic therapy. *Journal of colloid and interface science* **2022,** *617*, 704-717.

36. Elia, I.; Rossi, M.; Stegen, S.; Broekaert, D.; Doglioni, G.; van Gorsel, M.; Boon, R.; Escalona-Noguero, C.; Torrekens, S.; Verfaillie, C.; Verbeken, E.; Carmeliet, G.; Fendt, S.-M., Breast cancer cells rely on environmental pyruvate to shape the metastatic niche. *Nature* **2019,** *568* (7750), 117-121.

37. Yoo, H. C.; Yu, Y. C.; Sung, Y.; Han, J. M., Glutamine reliance in cell metabolism. *Experimental & Molecular Medicine* **2020,** *52* (9), 1496-1516.

38. Hö̈ckel, M.; Vaupel, P., Tumor Hypoxia: Definitions and Current Clinical, Biologic, and Molecular Aspects. *JNCI: Journal of the National Cancer Institute* **2001,** *93* (4), 266-276.

39. Ngamchuea, K.; Batchelor-McAuley, C.; Compton, R. G., The Copper(II)-Catalyzed Oxidation of Glutathione. *Chemistry – A European Journal* **2016,** *22* (44), 15937-15944.

40. Krebs, H. A., The effect of inorganic salts on the ketone decomposition of oxaloacetic acid. *Biochemical Journal* **1942,** *36* (3-4), 303-305.

41. Bansal, A.; Simon, M. C., Glutathione metabolism in cancer progression and treatment resistance. *The Journal of cell biology* **2018,** *217* (7), 2291-2298.

42. Frisch, M. J.; Trucks, G. W.; Schlegel, H. B.; Scuseria, G. E.; Robb, M. A.; Cheeseman, J. R.; Scalmani, G.; Barone, V.; Petersson, G. A.; Nakatsuji, H.; Li, X.; Caricato, M.; Marenich, A. V.; Bloino, J.; Janesko, B. G.; Gomperts, R.; Mennucci, B.; Hratchian, H. P.; Ortiz, J. V.; Izmaylov, A. F.; Sonnenberg, J. L.; Williams; Ding, F.; Lipparini, F.; Egidi, F.; Goings, J.; Peng, B.; Petrone, A.; Henderson, T.; Ranasinghe, D.; Zakrzewski, V. G.; Gao, J.; Rega, N.; Zheng, G.; Liang, W.; Hada, M.; Ehara, M.; Toyota, K.; Fukuda, R.; Hasegawa, J.; Ishida, M.; Nakajima, T.; Honda, Y.; Kitao, O.; Nakai, H.; Vreven, T.; Throssell, K.; Montgomery Jr., J. A.; Peralta, J. E.; Ogliaro, F.; Bearpark, M. J.; Heyd, J. J.; Brothers, E. N.; Kudin, K. N.; Staroverov, V. N.; Keith, T. A.; Kobayashi, R.; Normand, J.; Raghavachari, K.; Rendell, A. P.; Burant, J. C.; Iyengar, S. S.; Tomasi, J.; Cossi, M.; Millam, J. M.; Klene, M.; Adamo, C.; Cammi, R.; Ochterski,

J. W.; Martin, R. L.; Morokuma, K.; Farkas, O.; Foresman, J. B.; Fox, D. J. *Gaussian 16 Rev. C.01*, Wallingford, CT, 2016.

43. Alegre-Requena, J. V.; Shree, S. S. V.; Perez-Soto, R.; Alturaifi, T. M.; Paton, R. S., AQME: Automated quantum mechanical environments for researchers and educators. *Wires Comput Mol Sci* **2023**, e1663.

44. Landrum, G. Rdkit: Open-source cheminformatics software.

45. Becke, A. D., Density-functional thermochemistry. V. Systematic optimization of exchange-correlation functionals. *The Journal of Chemical Physics* **1997,** *107* (20), 8554-8560.

46. Chai, J.-D.; Head-Gordon, M., Long-range corrected hybrid density functionals with damped atom–atom dispersion corrections. *Physical Chemistry Chemical Physics* **2008,** *10* (44), 6615-6620.

47. Hehre, W. J.; Ditchfield, R.; Pople, J. A., Self—Consistent Molecular Orbital Methods. XII. Further Extensions of Gaussian—Type Basis Sets for Use in Molecular Orbital Studies of Organic Molecules. *The Journal of Chemical Physics* **2003,** *56* (5), 2257-2261.

48. Hariharan, P. C.; Pople, J. A., The influence of polarization functions on molecular orbital hydrogenation energies. *Theoretica chimica acta* **1973,** *28* (3), 213-222.

49. Krishnan, R.; Binkley, J. S.; Seeger, R.; Pople, J. A., Self-consistent molecular orbital methods. XX. A basis set for correlated wave functions. *The Journal of Chemical Physics* **2008,** *72* (1), 650-654.

50. McLean, A. D.; Chandler, G. S., Contracted Gaussian basis sets for molecular calculations. I. Second row atoms, Z=11–18. *The Journal of Chemical Physics* **2008,** *72* (10), 5639-5648.

51. Francl, M. M.; Pietro, W. J.; Hehre, W. J.; Binkley, J. S.; Gordon, M. S.; DeFrees, D. J.; Pople, J. A., Self-consistent molecular orbital methods. XXIII. A polarization-type basis set for second-row elements. *The Journal of Chemical Physics* **1982,** *77* (7), 3654-3665.

52. Weigend, F.; Ahlrichs, R., Balanced basis sets of split valence, triple zeta valence and quadruple zeta valence quality for H to Rn: Design and assessment of accuracy. *Physical Chemistry Chemical Physics* **2005,** *7* (18), 3297-3305.

53. Weigend, F., Accurate Coulomb-fitting basis sets for H to Rn. *Physical Chemistry Chemical Physics* **2006,** *8* (9), 1057-1065.

54. Cancès, E.; Mennucci, B.; Tomasi, J., A new integral equation formalism for the polarizable continuum model: Theoretical background and

applications to isotropic and anisotropic dielectrics. *The Journal of Chemical Physics* **1997,** *107* (8), 3032-3041.

55. Mennucci, B.; Cancès, E.; Tomasi, J., Evaluation of Solvent Effects in Isotropic and Anisotropic Dielectrics and in Ionic Solutions with a Unified Integral Equation Method: Theoretical Bases, Computational Implementation, and Numerical Applications. *The Journal of Physical Chemistry B* **1997,** *101* (49), 10506-10517.

56. Mennucci, B.; Tomasi, J., Continuum solvation models: A new approach to the problem of solute's charge distribution and cavity boundaries. *The Journal of Chemical Physics* **1997,** *106* (12), 5151-5158.

57. Tomasi, J.; Mennucci, B.; Cancès, E., The IEF version of the PCM solvation method: an overview of a new method addressed to study molecular solutes at the QM ab initio level. *Journal of Molecular Structure: THEOCHEM* **1999,** *464* (1), 211-226.

58. Scalmani, G.; Frisch, M. J., Continuous surface charge polarizable continuum models of solvation. I. General formalism. *The Journal of Chemical Physics* **2010,** *132* (11).

59. Marenich, A. V.; Cramer, C. J.; Truhlar, D. G., Universal Solvation Model Based on Solute Electron Density and on a Continuum Model of the Solvent Defined by the Bulk Dielectric Constant and Atomic Surface Tensions. *The Journal of Physical Chemistry B* **2009,** *113* (18), 6378-6396.

60. Luchini, G.; Alegre-Requena, J.; Funes-Ardoiz, I.; Paton, R. S. J. F., GoodVibes: automated thermochemistry for heterogeneous computational chemistry data. *F1000Research* **2020**, *9*, 291.

61. DeBerardinis, R. J.; Mancuso, A.; Daikhin, E.; Nissim, I.; Yudkoff, M.; Wehrli, S.; Thompson, C. B., Beyond aerobic glycolysis: Transformed cells can engage in glutamine metabolism that exceeds the requirement for protein and nucleotide synthesis. **2007,** *104* (49), 19345-19350.

62. Nelson, D. L.; Lehninger, A. L.; Cox, M. M., *Lehninger Principles of Biochemistry*. W. H. Freeman: 2008.

63. Tardito, S.; Oudin, A.; Ahmed, S. U.; Fack, F.; Keunen, O.; Zheng, L.; Miletic, H.; Sakariassen, P. Ø.; Weinstock, A.; Wagner, A.; Lindsay, S. L.; Hock, A. K.; Barnett, S. C.; Ruppin, E.; Mørkve, S. H.; Lund-Johansen, M.; Chalmers, A. J.; Bjerkvig, R.; Niclou, S. P.; Gottlieb, E., Glutamine synthetase activity fuels nucleotide biosynthesis and supports growth of glutamine-restricted glioblastoma. *Nature Cell Biology* **2015,** *17* (12), 1556-1568.

64. Altman, B. J.; Stine, Z. E.; Dang, C. V., From Krebs to clinic: glutamine metabolism to cancer therapy. *Nature Reviews Cancer* **2016,** *16* (10), 619-634.

65. Goerigk, L.; Grimme, S., A thorough benchmark of density functional methods for general main group thermochemistry, kinetics, and noncovalent interactions. Phys. *Chem. Chem. Phys*. **2011**, *13*, 6670–6688.

66. The PyMOL Molecular Graphics System, version 2.0.7, Schrödinger, LLC.

67. https://gist.github.com/bobbypaton (accessed 09 July 2021).

68. Grimme, S., Supramolecular Binding Thermodynamics by Dispersion-Corrected Density Functional Theory. *Chem. Eur. J*. **2012**, *18*, 9955–9964